

Design, Synthesis and Pharmacological Evaluation of Second Generation EZH2 Inhibitors with Long Residence Time

Avinash Khanna, Alexandre Côté, Shilpi Arora, Ludivine Moine, Victor S Gehling, Jehrod Brenneman, Nico Cantone, Jacob I Stuckey, Shruti Apte, Ashwin Ramakrishnan, Kamil Bruderek, William D. Bradley, James E. Audia, Richard T. Cummings, Robert J. Sims, Patrick Trojer, and Julian R. Levell

ACS Med. Chem. Lett., **Just Accepted Manuscript** • DOI: 10.1021/acsmchemlett.0c00045 • Publication Date (Web): 26 Mar 2020

Downloaded from pubs.acs.org on March 27, 2020

Just Accepted

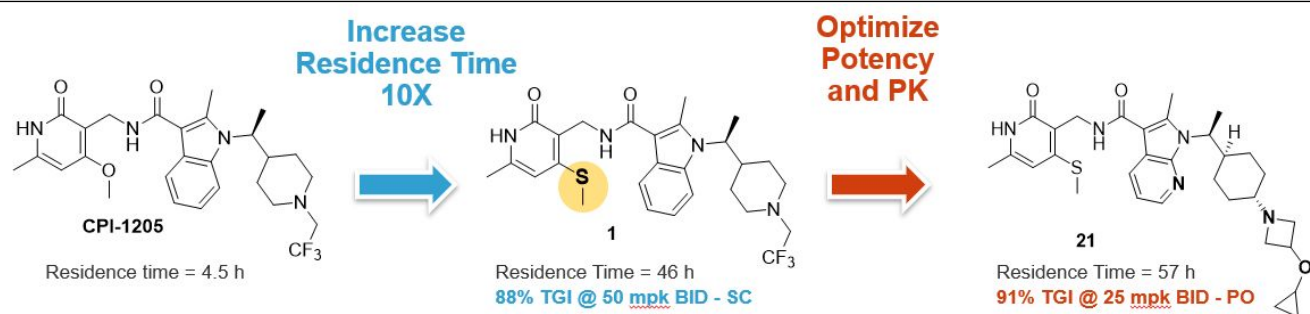
"Just Accepted" manuscripts have been peer-reviewed and accepted for publication. They are posted online prior to technical editing, formatting for publication and author proofing. The American Chemical Society provides "Just Accepted" as a service to the research community to expedite the dissemination of scientific material as soon as possible after acceptance. "Just Accepted" manuscripts appear in full in PDF format accompanied by an HTML abstract. "Just Accepted" manuscripts have been fully peer reviewed, but should not be considered the official version of record. They are citable by the Digital Object Identifier (DOI®). "Just Accepted" is an optional service offered to authors. Therefore, the "Just Accepted" Web site may not include all articles that will be published in the journal. After a manuscript is technically edited and formatted, it will be removed from the "Just Accepted" Web site and published as an ASAP article. Note that technical editing may introduce minor changes to the manuscript text and/or graphics which could affect content, and all legal disclaimers and ethical guidelines that apply to the journal pertain. ACS cannot be held responsible for errors or consequences arising from the use of information contained in these "Just Accepted" manuscripts.

Design, Synthesis and Pharmacological Evaluation of Second Generation EZH2 Inhibitors with Long Residence Time

Avinash Khanna[‡], Alexandre Côté[‡], Shilpi Arora, Ludivine Moine, Victor S. Gehling, Jehrod Brenneman, Nico Cantone, Jacob I. Stuckey, Shruti Apte, Ashwin Ramakrishnan, Kamil Bruderek, William D. Bradley, James E. Audia, Richard T. Cummings, Robert J. Sims III, Patrick Trojer, Julian R. Levell

Constellation Pharmaceuticals 215 First St. Suite 200, Cambridge MA, 02142

KEYWORDS: Residence time, EZH2, thiomethyl pyridone, CYP induction



ABSTRACT: Histone methyltransferase EZH2, which is the catalytic subunit of the PRC2 complex, catalyzes the methylation of histone H3K27 - a transcriptionally repressive post-translational modification (PTM). EZH2 is commonly mutated in hematologic malignancies and frequently overexpressed in solid tumors, where its expression level often correlates with poor prognosis. 1st generation EZH2 inhibitors are beginning to show clinical benefit, and we believe that a 2nd generation EZH2 inhibitor could further build upon this foundation to fully realize the therapeutic potential of EZH2 inhibition. During our medicinal chemistry campaign, we identified 4-thiomethyl pyridone as a key modification that led to significantly increased potency and prolonged residence time. Leveraging this finding, we optimized a series of EZH2 inhibitors, with enhanced anti-tumor activity and improved physiochemical properties, which have the potential to expand the clinical use of EZH2 inhibition.

Polycomb repressive complex 2 (PRC2) is responsible for the tri-methylation of lysine 27 on histone 3 (H3K27), a modification which serves to repress transcription[1]. Enhancer of zeste homologue 2 (EZH2), a subunit of PRC2, catalyzes the transfer of a methyl group from the co-factor *S*-adenosyl-L-methionine (SAM) to the ϵ -NH₂ group of H3K27 culminating in trimethylation of H3K27 (H3K27Me₃)[2] and subsequent silencing of targeted genes[3]. The dysregulation of target genes by the “trimethylation marks” has been implicated in a variety of disease processes, particularly oncogenesis[4, 5].

EZH2 has been reported to be mutated or overexpressed in a broad spectrum of oncology indications such as prostate cancer[6], lung cancer[7], myeloma, and lymphoma[8]. Furthermore, activating mutations in EZH2 have been shown to be a key driver of diffuse large B-cell lymphoma and follicular lymphoma[9], while resistance to hormone therapy has been shown to arise from upregulation of EZH2 expression in prostate cancer[6]. The increased levels of

H3K27Me₃ that result from EZH2 upregulation reinforce the silencing of target genes, which promote differentiation and restrain proliferation in normal cells[10]. Clinical EZH2 inhibitors (Figure 1) are currently being evaluated as monotherapy and in combination in both hematological malignancies and solid tumors, including specific genomic contexts such as mutations in EZH2 and components of SWItch/Sucrose non-fermentable (SWI/SNF) – a nucleosome remodeling complex (NCT03213665). Initial results in the clinic have further validated the role of EZH2 catalytic activity in the context of follicular lymphoma, where patients with activating mutations respond at a higher rate to EZH2 inhibitors than those with wild-type EZH2 [11].

EZH2 inhibitors in the clinic have been reported to exhibit favorable safety profiles and display anti-tumor activity, particularly in hypersensitive contexts, such as lymphoma, and in combination [12]. Initial dose escalation studies have resulted in recommended phase 2 doses of >800 mg BID [13]. Even though clinical agents have thus far been found to be well-tolerated, significant reduction in exposure is observed after multiple dosing in humans [12, 14], consistent with induction of CYP3A4 leading to faster metabolism of the drug [11], [15]. The high dose and CYP induction present potential limitations when including first generation EZH2 inhibitors as part of a combination therapy. Furthermore, our preclinical data showed that prolonged treatment is necessary to trigger a decrease in H3K27Me3, in agreement with the slow turnover kinetics of histone H3K27Me3 modification. To maximize the oncology application potential of EZH2 inhibition in the clinic, we initiated a 2nd generation program that sought to achieve increased and more durable target coverage.

the active site as the SAM co-factor (Figure 1) [16] [17]. In particular, the amino acid moiety of either SAM or *S*-adenosylhomocysteine (SAH), and the pyridone motif of the EZH2 inhibitors overlap (highlighted in Figure 1). The pyridone competes with the co-factor for the H-bond donor-acceptor interaction with tryptophan 624. Specifically, the N-H of the pyridone serves as an H-bond donor for the peptide-backbone's carbonyl oxygen. Accordingly, we surmised that favoring the compound's tautomer population towards the pyridone over the hydroxypyridine would lead to more potent EZH2 inhibitors. This analysis suggested to us that the electronic nature of the pyridone, electron-rich or -poor, would be highly critical for the inhibitor's potency for EZH2. Therefore, using our CPI-1205 indole scaffold as a starting point we generated a variety of substituted pyridones, including compounds 1-5 (Figure 2). The biochemical potencies of these inhibitors were found to be in the range of 30 nM to 0.2 nM, and their comparison showed that heteroatom substitution was

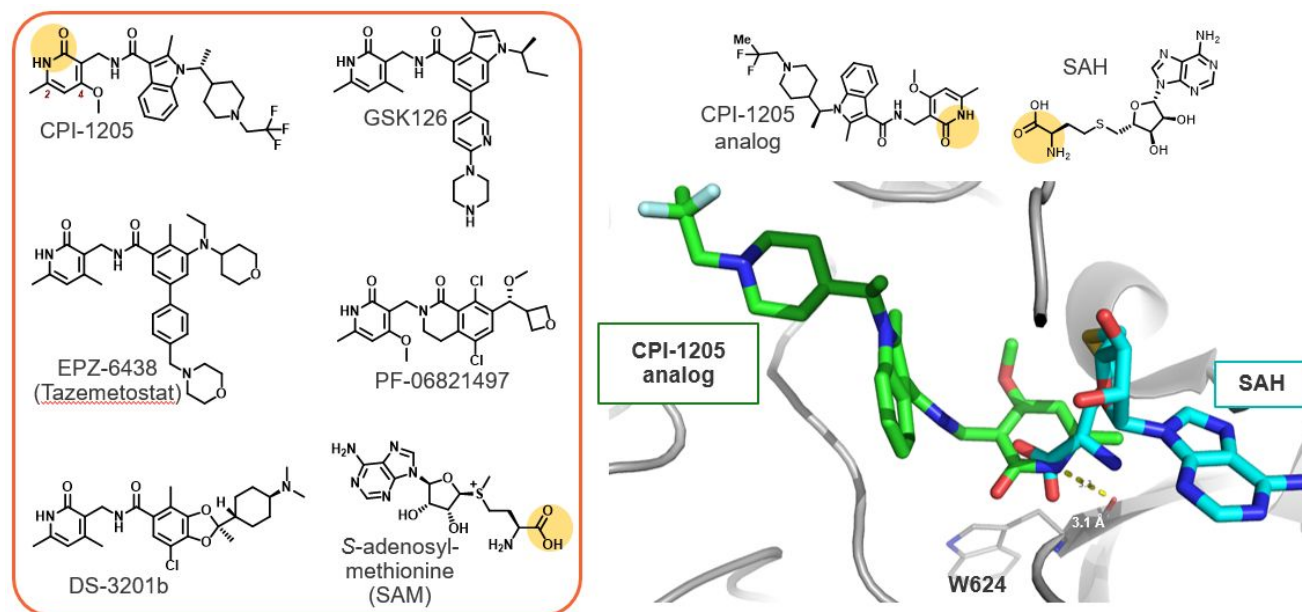
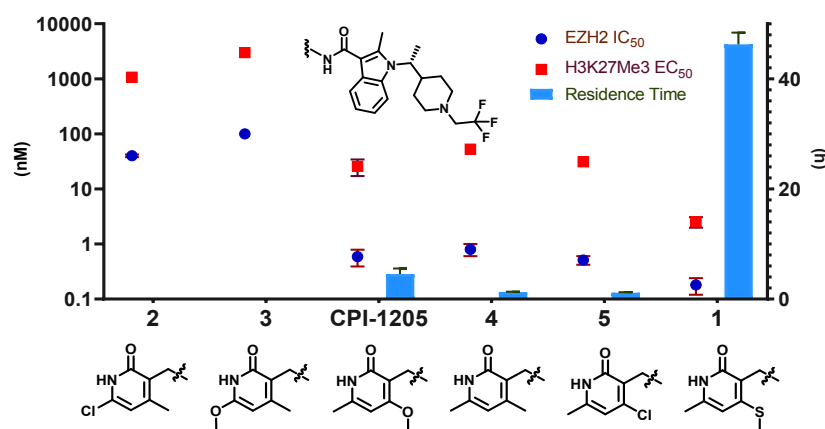


Figure 1. *Left*: Clinical inhibitors of EZH2 and *S*-adenosyl-methionine, the endogenous co-factor of EZH2. *Right*: Overlay of SAH (*S*-adenosylhomocysteine) in cyan bound to EZH2 (grey) and a CPI-1205 analog (green), with the structures of the ligands depicted above.

We initiated our medicinal chemistry campaign with an analysis of inhibitor bound EZH2 co-crystal structures, which

preferred at the 4-position over the 2-position, with the 4-thiomethyl-pyridone exhibiting the lowest IC₅₀. The rank



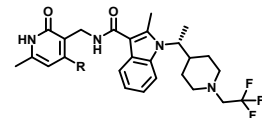
showed that the pyridone moiety occupies the same pocket of

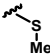
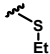
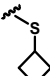
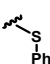
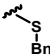
ordering of pyridone biochemical potencies also correlated well

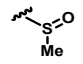
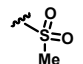
Figure 2. TR-FRET and MSD based EZH2 inhibition assay, and TR-FRET based residence time characterization.

with their activity in the cellular H3K27Me3 level reduction assay. Inhibitors **2** and **3**, which feature a 2-chloro and a 2-methoxy pyridone, respectively, were found to have cellular

Table 1: Optimization of 4-thioether pyridone



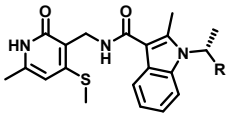
Cmpd	R	IC ₅₀ ^a (nM)	H3K27Me3 EC ₅₀ ^a (nM)
1		0.18 (0.06)	2.5 (0.54)
6		0.73 (0.04)	45.3
7		0.49 (0.04)	48.5
8		0.62 (0.2)	181
9		3.8 (0.5)	-

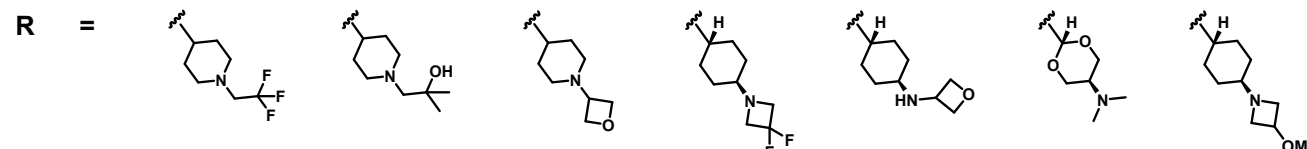
10		19 (6)	>304
11		4.1 (0.4)	>304

^a Average with the standard deviation reported in parentheses, where $n \geq 2$.

EC₅₀s of >1 μM. Whereas, the inhibitors that feature heteroatoms at the 4-position, such as **5**, **1** and **CPI-1205** were found to exhibit cellular EC₅₀'s of <100 nM. In particular, the 4-thiomethyl pyridone **1** was found to be the most potent in both the biochemical and the cellular H3K27Me3 mark reduction assays (EC₅₀ = 2.5 nM). Due to the over-performance of **1** in the cellular assay, we sought to characterize the residence time of the more active analogs, **4**, **5**, **1** and **CPI-1205**. We found that, although their biochemical potencies were in a similar range (180 pM - 800 pM), the thiomethyl pyridone **1** exhibited a distinctly longer residence time. More starkly, **1** exhibits nearly a 10-fold greater residence time than its oxygen analog, **CPI-1205** (Figure 1), in agreement with a 10-fold improvement in both the H3K27Me3 EC₅₀ and the GI₅₀ (KARPAS-422 lymphoma cells).[18] Note, we also tested the 2-thiomethyl, 4-methyl substituted pyridone analog and found it to be inactive in the biochemical assay, similar to compound **3**.

Table 2. Optimization of piperidine sidechain^a



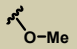
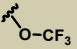
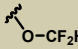
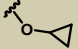
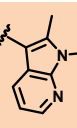
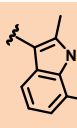
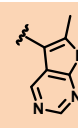
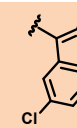
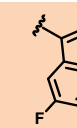
R = 

Cmpd	1	12	13	14	15	16	17
EZH2 IC ₅₀ (nM)	0.18 (0.06)	0.067 (0.01)	0.12 (0.007)	0.18 (0.03)	0.13 (0.02)	0.16 (0.01)	0.059 (0.01)
H3K27Me3 EC ₅₀ (nM)	2.5 (0.54)	26	5.1	5.9 (2.0)	6.7 (2.81)	2.4 (0.58)	2.0 (0.49)
CYP3A4 UpReg @ 10 μM	25X (3.5)	-	6.4X (1.0)	45X (1.9)	5X (0.79)	3X (0.18)	2X (0.12)
cLogD	3.8	2.9	3.2	3.8	3.0	2.3	3.3
τ (h)	46.3 (2.1)	7.52 (0.45)	42.5 (0.45)	29.1 (0.05)	138 (5.0)	40.9 (4.5)	141 (8.8)

^a Average with the standard deviation reported in parentheses, where $n \geq 2$.

Table 3. Optimization of piperidine sidechain and indole-core



									
Cmpd	17	18	19	20	21	22	23	24	25
EZH2 IC ₅₀ ^a (nM)	0.059 (0.01)	0.14 (0.02)	0.10 (0.03)	0.072 (0.05)	0.057 (0.009)	0.063 (0.01)	0.10 (0.01)	0.092 (0.04)	0.060 (0.0004)
H3K27Me 3 EC ₅₀ (nM)	2.0 (0.49)	1.8 (0.01)	0.7 (0.13)	3.5	1.8 (0.5)	3.4	6.3 (0.9)	3.5 (0.5)	1.8 (0.4)
CYP3A4 Up-Reg @ 10 μM	2X (0.12)	41X (0.03)	32X (0.4)	17X (0.01)	2.2X (0.002)	-	-	1.6X (0.01)	12X (0.3)
cLogD	3.2	3.6	4.0	3.5	3.2	3.6	2.8	3.7	3.2
KARPAS- 422 GI ₅₀ (nM)	33	32	12 (1.3)	13	12	32	29	37 (4.4)	24 (3.4)
τ (h)	141 (8.8)	-	211 (29)	289 (22)	57.5 (5.2)	100 (2.7)	51.9 (1.9)	64.2 (5.2)	65.8 (1.2)

^a Average with the standard deviation reported in parentheses, where $n \geq 2$.

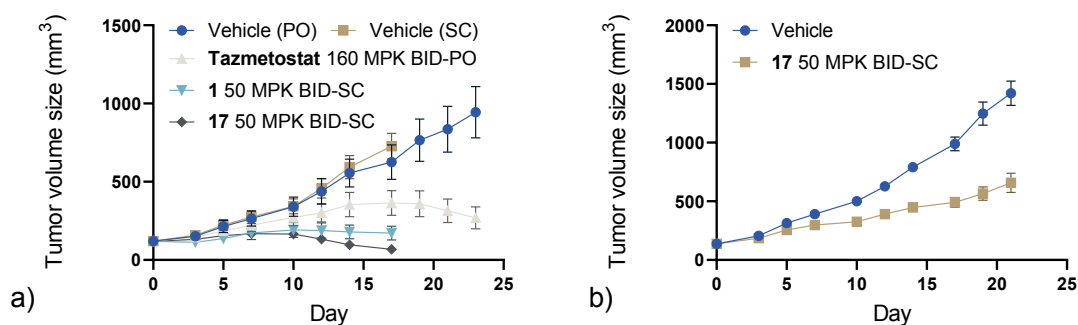


Figure 3. a) Evaluation of **1** and **17** in KARPAS-422 lymphoma xenograft mouse model. b) Evaluation of **17** in 22Rv1 prostate cancer xenograft mouse model

Having identified a novel pyridone motif that engenders increased residence time and cellular potency, we generated a series of 4-thioalkyl substituted pyridones, **6–11** (Table 1). We found that increasing the substituent size (**6–9**) led to a decrease in potency. Likewise, oxidation of the thioether to a methylsulfinyl or a methylsulfone led to an even greater decrease in potency. Given the large drop in the biochemical potency, we did not characterize the residence time for this series. The 4-thiomethyl substituent, exemplified in **1**, was found to be the most potent EZH2 inhibitor. We have applied this finding to many other clinical EZH2 scaffolds by replacing their pyridone with the 4-thiomethylpyridone of **1** and found a similar increase in inhibitor residence time (8 – 23 fold)[19]. We hypothesize that the superiority of the 4-thiomethyl substitution is due to a combination of multiple factors, including: i) pyridone:hydroxypyridine tautomeric ratio; ii) the larger van der Waal's radius of sulfur which leads to a larger hydrophobic buried surface area; iii) the tighter methyl contact with the protein due to larger C-S bond lengths; and possibly iv) a positive S- π interaction with the electron rich sidechains of phenylalanines 665 and 686.[20]

Being conscious of the previously reported CYP3A4 induction, we sought to characterize the propensity of **1** to induce expression of the cytochrome p450 enzyme CYP3A4. Therefore, we treated the immortalized human hepatocytes, Fa2N-4 cells with 10 μM of **1** and found nearly a 25-fold increase in the expression of CYP3A4 [21]. With the 4-thiomethyl-pyridone motif in place, we sought to optimize the piperidine sidechain to further enhance potency and to limit CYP3A4 upregulation. We found that introduction of beta-oxygenation led to a decrease in CYP3A4 upregulation (**12** and **13**), however this also led to a decrease in biochemical potency (Table 2). The potency was enhanced by replacing the piperidine with an exocyclic amine, as in **14** and **17**. Further characterization of compound mediated CYP3A4 upregulation showed that **17** only upregulated CYP3A4 2-fold, in comparison to 25-fold with **1**. SAR of the piperidine sidechain showed a correlation between cLogD and CYP3A4 upregulation, where the compounds with lower cLogD exhibited limited CYP3A4 upregulation (Table 2)[22]. We determined that a 2-fold increase of CYP3A4 expression, under our assay conditions of 10 μM compound treatment, would be sufficient for progressing the program given that we do not anticipate

achieving such high concentrations *in vivo*. As a result, by elaborating from **1** to **17**, we improved biochemical potency, retained cellular activity, enhanced residence time and limited *CYP3A4* upregulation.

Table 4: *In vitro* and *in vivo* characterization of **1**, and **21**

Assay	1	21
EZH2 IC ₅₀ (nM)	0.18	0.057
H3K27Me3 EC ₅₀ (nM)	2.5	1.8
cLogD (StarDrop)	3.8	3.1
<i>CYP3A4</i> UpReg @ 10 μM	25X	2.2X
KARPAS-422 GI ₅₀ (8 days) (nM)	N/A	12.2
τ (h)	46.3	57.5
Mouse IV Clearance (L/h/Kg)	0.56	3.35
Mouse oral bioavailability - F (%)	40	15
AUC _{last/D} (h*mg/mL)	414.4	46.5
Plasma Protein Binding - m, h	99.8, 97	87, 97
KARPAS-422 %TGI	77 @ 50 MPK BID-SC	91 @ 25 MPK BID-PO

Given the improvements in potency and limited *CYP3A4* upregulation, we sought to characterize **1** and **17** in the KARPAS-422 lymphoma xenograft mouse model (Figure 3). A 160 mg/kg BID - PO dose of Tazemetostat, which has previously been shown to cause regression in this model[23], was used as a benchmark compound in the study. With the goal of rank-ordering compounds for our medicinal chemistry campaign, we kept the BID dosing regimen constant during our *in vivo* studies and evaluated efficacy and kinetics of achieving regression. We dosed inhibitors at 50 mg/kg BID, which we hypothesized would provide a dynamic range of efficacy between compounds. **1** and **17**, which were both dosed SC, began to cause regression at days 7 and 9, respectively, a marked improvement over the benchmark. To ensure enough tumor sample could be obtained for downstream characterization, mice in the treatment arms of **1** and **17** were sacrificed after 17 days (no body weight loss observed, see

supplemental). Meanwhile, **Tazemetostat** was dosed out to day 24 to ensure the benchmark compound also achieved regression.

We then characterized the efficacy of **17** in the 22Rv1 prostate cancer xenograft model in mice. 22Rv1 cells have been shown to express high levels of EZH2 when compared to other prostate cancer cell models, and they are dependent on androgen receptor signaling for growth [24]. The 22Rv1 cell-line is not sensitive to androgen-degrader therapies such as Enzalutamide because it expresses the AR-V7 isoform of the androgen-receptor, which lacks the ligand-binding domain[25]. We found that a 50 mg/kg BID - SC dose of **17** led to ~ 55% TGI.

Although **17** achieved *in vivo* efficacy in both models, it was not orally bioavailable, therefore we next sought to improve upon the inhibitor's physiochemical properties. We hypothesized that the methoxy substituent was not lipophilic enough to mask to heightened basicity of azetidine **17**, this potentially led to decreased absorption[16]. We replaced the methyl group of the azetidinol with substituents that would mitigate the basicity of the exocyclic amine, such as fluoroalkyls **18**, and **19**. We also replaced the methyl group of the azetidinol with a cyclopropane in **20** to increase the lipophilicity, and in-turn improve permeability. Through these modifications we found that the methyl to cyclopropyl replacement resulted in a 3-fold improvement in GI₅₀ (**17** vs. **20**). Although these modifications led to increased potency, particularly in the cellular proliferation assays, as seen with **19** and **20**, they also resulted in an increase of *CYP3A4* upregulation, potentially due to their higher clogD. To combat *CYP3A4* upregulation, we retained the cyclopropoxy sidechain of **20** and introduced heteroatoms within the central indole-core to increase polarity. In particular, we introduced a nitrogen within the central core to generate aza-indole **21**, which retained many of the desirable properties of **17** such as cellular potency and decreased *CYP3A4* upregulation (~5 fold **20** vs. **21**). Replacing the aza-indole in **21** with a fluoro-indole in **22** led to diminished activity in the cellular assays, including the cell proliferation assay. We also generated the pyrrolopyrimidine **23** in an effort to decrease the clogD, however this further led to loss in cellular activity. 5-halosubstituted aza-indoles **24** and **25** were found to be less active in the cellular assays, and, in the case of **25**, led to a greater *CYP3A4* upregulation than **21**. Unlike the clear correlation observed with our earlier sidechain modifications (Table 2), we did not observe a strict correlation of clogD with *CYP3A4* upregulation in the case of compounds **20-25**. Nevertheless, during this survey we identified **21**, an aza-indole which provided a balance of favorable properties such as improved potency, and negligible *CYP3A4* upregulation, while also exhibiting 15% oral bioavailability (Table 4).

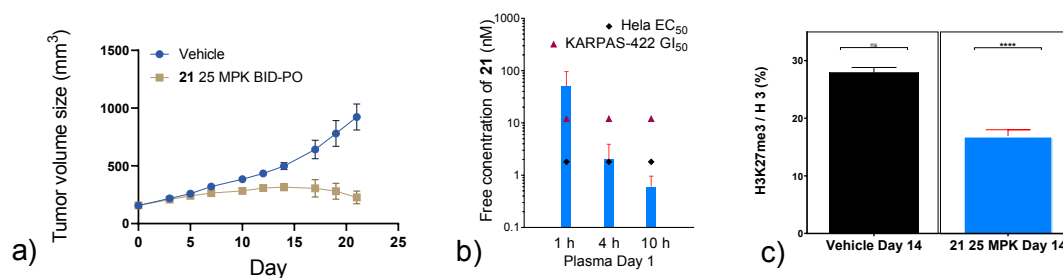
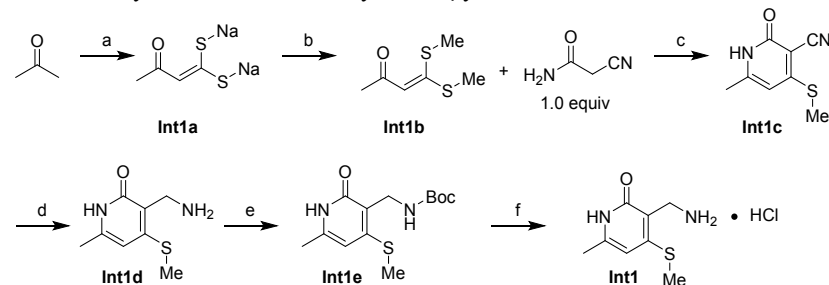


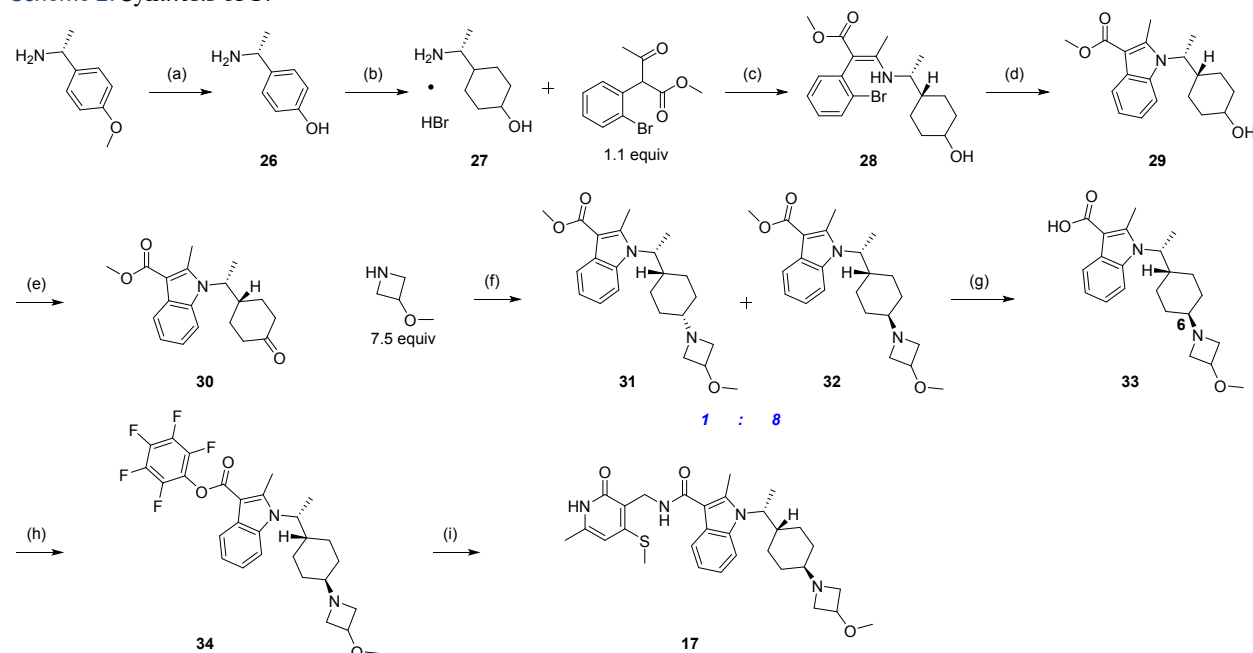
Figure 4. a) Evaluation of **21** in KARPAS-422. b) Pharmacokinetics of **21** at day 1 of treatment. c) Modulation of H3K27me3 pharmacodynamic marker upon treatment for 14 days

Scheme 1. Synthesis of 4-thiomethyl aminopyridone Int1^a



^aReagents and conditions: (a) t-BuONa (2 equiv), CS₂ (1.0 equiv), toluene, 0 °C, 4 h; (b) MeI (2.0 equiv), MeOH, 70 °C, 1 h (42% yield over two steps); (c) t-BuONa, t-BuOH, 80 °C, 12 h (75% yield); (d) BH₃-Me₂S (4.0 equiv), THF, 70 °C, 2 h; (e) Boc₂O (3.0 equiv), Et₃N (1.5 equiv), THF, 25 °C, 12 h (75% yield over two steps); (f) HCl, MeOH, 70 °C, 2 h.

Scheme 2. Synthesis of 17^a



^aReagents and conditions: (a) HBr (35% in AcOH), 100 °C, 12 h; (b) PtO₂ (0.05 equiv), H₂ (55 psi), AcOH (1.5 equiv), MeOH, 50 °C, 30 h; (c) MeONa (1.1 equiv), MeOH, 25 °C, 1 h then ketoester (1.1 equiv), AcOH (1.3 equiv), tBuOH, 85 °C, 12 h (7.6% yield over 3 steps); (d) RuPhos precatalyst (generation 2) (10 mol %), dioxane, 100 °C, 13 h (88% yield); (e) Dess-Martin reagent (2.0 equiv), DCM, 10 °C, 16 h (77% yield); (f) iPr₂NEt (8.3 equiv), MeOH, 25 °C, 1 h then **30** (1.0 equiv), THF, 25 °C, 2 h then LiBH₄ (1.4 equiv), -70 °C, 15 min (45% yield for desired diastereomer); (g) NaOH (10.0 equiv), MeOH, H₂O, 80 °C, 12 h; (h) perfluorophenyl 2,2,2-trifluoroacetate (1.5 equiv), pyridine (2 equiv), DCM, 25 °C; (i) **Int1** (3.0 equiv), iPr₂NEt (3.0 equiv), DMF, 25 °C, 12 h (31% yield over 2 steps)

Next, we profiled **21** in the KARPAS-422 lymphoma mouse model at 25 mg/kg BID – PO, which is nearly a 6-fold lower dose than the benchmark in figure 3. In this study, we

found that the tumors began to regress at day 14 and resulted in TGI of 75% by day 21, with no impact on mouse body weight (see supplemental information). Unbound plasma levels of **21**

were found to be above H3K27Me3 mark reduction assay EC₅₀ in the tumors for 4 hours. Tumor PD experiments showed that H3K27Me3 mark was significantly decreased at day 14 (Figure 4). The oxidative metabolic stability for **21** was not characterized in metabolic liability identification studies. However, we did not observe **10** or **11** during mouse PK experiments of **1**.

In summary, the goal of our second generation EZH2 medicinal chemistry campaign was to improve target coverage, and to limit *CYP3A4* upregulation. Starting with a reassessment of the binding interaction of the inhibitor and EZH2, we identified the 4-thiomethyl substituent as a key modification for the enhancement of potency and residence time in **1**. We then tackled the challenge of retaining the improved cellular potency and limiting *CYP3A4* upregulation through the identification of an exocyclic azetidine sidechain in **17**. As a result, we were able to expand the utility of an EZH2 inhibitor to an enzalutamide-resistant prostate cancer mouse model (22Rv1). Although **17** provided impressive efficacy, it was not orally bioavailable. Therefore, we replaced the indole-core with a set of heterocycles, which led to the discovery of **21**.

Aza-indole **21** was found to be a highly efficacious EZH2 inhibitor, achieving >91% TGI in 25 days with the oral dose of 25 mg/kg BID – PO. Pharmacokinetic (PK) and pharmacodynamic (PD) profiling showed that the exposure levels of **21** were sustained above cellular EC₅₀ for 4 hours and the level of H3K27Me3 mark reduction was also maintained. The discovery of the 4-thiomethyl pyridone modification and its ability to bestow durable target coverage was a key stepping-stone to developing 2nd generation EZH2 inhibitors.

Chemistry

We took advantage of the well-precedented peptide coupling of the aminopyridone and the indole acid to synthesize most of the compounds included in this report[16]. The 4-thioether amino-pyridones were synthesized by adapting the route from scheme 1, while the 6-methoxy and 6-chloropyridones were synthesized via the 6-hydroxypyridone

Supporting Information

The Supporting Information is available free of charge on the ACS Publications website.

Methods and Materials, Biochemical and Cellular Assay Procedures, Experimental Details for *In Vivo* Experiments, Synthetic Experimental Details, and Compound Purity Assessment

AUTHOR INFORMATION

Corresponding Author

* Avinash Khanna: Avinash.khanna@constellationpharma.com. Tel. (617) 714-0556

Present Addresses

†Alexandre Côté (Schrödinger Inc., New York, NY), ‡Shilpi Arora (X-Chem Inc. Waltham, MA), †Ludivine Moine (Blueprint Medicines, Cambridge, MA), †Jehrod Brenneman (KSQ Therapeutics, Cambridge, MA), †Jacob I. Stuckey (Third Rock Ventures, Boston, MA), †Shruti Apte (X-Chem Inc. Waltham, MA), †Ashwin Ramakrishnan (BMS, Cambridge, MA), †Kamil Bruderek (Relay Therapeutics, Cambridge, MA), †William D. Bradley (Cyteir Therapeutics, Lexington, MA), †James E. Audia (Third Rock Ventures, Boston, MA), †Robert J. Sims III (Third Rock Ventures, Boston, MA)

Author Contributions

The manuscript was written through contributions of all authors. / All authors have given approval to the final version of the manuscript. / ‡These authors contributed equally. (match statement to author names with a symbol)

Funding Sources

Any funds used to support the research of the manuscript should be placed here (per journal style).

carbonitrile (see supplemental). The synthesis of the 4-thiomethylaminopyridone intermediate **1** commenced by condensing carbon disulfide onto acetone to give sodium bithiolate **Int1a**. The thiolates were then capped with methyl iodide to provide thioacetal **Int1b**, which was subjected to an aldol condensation reaction with 2-cyanoacetamide, that results in eventual cyclization under thermal conditions to provide cyanopyridone **Int1c**. The resulting nitrile was reduced to the primary amine, which was protected with Boc anhydride to simplify its purification and isolation (24% yield from acetone). Subsequent protecting group removal with hydrochloric acid resulted in a bench-top stable salt (>6 months) of 4-thiomethyl aminopyridone **Int1**.

Compounds containing the trifluoroethylpiperidine sidechain were synthesized using the general scheme previously described [16] (see supplemental for synthesis of pyridones). The synthesis of **17** (Scheme 2) began with demethylation of the commercial (*R*)-*p*-methoxybenzylamine, followed by its reduction, using PtO₂ at 55 psi of H₂, to aminoalcohol **27**. The aminoalcohol was then condensed with the bromoketoester to generate enamine **28**, and subsequently cyclized to furnish the indole with the RuPhos precatalyst (Gen II) in 88% yield. Cyclohexanol **29**, was oxidized to ketone **30**, which also served as a key intermediate for **14-15**, and **18-20**.

The methoxyazetidine was appended via reductive amination using a two-step procedure of imine formation and reduction with lithium borohydride, which provided the desired diastereomer in an 8:1 ratio (use of sodium cyanoborohydride led to a 1:1 mixture of both diastereomers). The two diastereomers were readily separated by column chromatography. The desired diastereomer, **32**, was hydrolyzed and activated as a perfluorophenyl (PFP) ester then directly treated with the aminopyridone **Int1** to give **17**.

ASSOCIATED CONTENT

ABBREVIATIONS

PTM, Post-translational modification; PRC2, polycomb repressive complex 2; H3K27, histone 3 lysine 27; EZH2, enhancer of zeste homologue 2; SWI/SNF, SWItch/Sucrose non-fermentable; SAM, Sadenosyl-L-methionine; PD, pharmacodynamics; cLogD, calculated LogD; SAR, structure activity relationships; PK, pharmacokinetic; SC, sub-cutaneous; IV, intravenous; PO, per os; F, bioavailability; DMA, dimethylacetamide; PEG, polyethylene glycol; iPrNet2, hunig's base; CDI, carbonyldiimidazole; THF, tetrahydrofuran; TGI, tumor-growth inhibition; BID, twice a day; QD, once a day; m, mouse; h, human; PtO₂, platinum oxide; PFP, perfluorophenyl

References

- Schuettengruber, B. and G. Cavalli, *Recruitment of Polycomb group complexes and their role in the dynamic regulation of cell fate choice*. Development, 2009. **136**(21): p. 3531-3542.
- Kadoch, C., R.A. Copeland, and H. Keilhack, *PRC2 and SWI/SNF Chromatin Remodeling Complexes in Health and Disease*. Biochemistry, 2016. **55**(11): p. 1600-1614.
- Margueron, R. and D. Reinberg, *The Polycomb complex PRC2 and its mark in life*. Nature, 2011. **469**(7330): p. 343-349.
- Bracken, A.P., et al., *Genome-wide mapping of Polycomb target genes unravels their roles in cell fate transitions*. Genes Dev, 2006. **20**(9): p. 1123-36.
- Yamaguchi, H. and M.-C. Hung, *Regulation and Role of EZH2 in Cancer*. Cancer Res Treat, 2014. **46**(3): p. 209-222.
- Ku, S.Y.e.a., *Rb1 and Trp53 cooperate to suppress prostate cancer lineage plasticity, metastasis, and antiandrogen resistance*. Science, 2017. **355**: p. 78-83.
- Sato, T., et al., *PRC2 overexpression and PRC2-target gene repression relating to poorer prognosis in small cell lung cancer*. Scientific Reports, 2013. **3**: p. 1911.
- Bodor, C., et al., *EZH2 Y641 mutations in follicular lymphoma*. Leukemia, 2011. **25**(4): p. 726-9.
- Morin, R.D., et al., *Somatic mutations altering EZH2 (Tyr641) in follicular and diffuse large B-cell lymphomas of germinal-center origin*. Nat Genet, 2010. **42**(2): p. 181-5.
- Gardner, E.E., et al., *Chemosensitive Relapse in Small Cell Lung Cancer Proceeds through an EZH2-SLFN11 Axis*. Cancer Cell, 2017. **31**(2): p. 286-299.
- Morschhauser, F.e.a. *Interim Report From a Phase 2 Multicenter Study of Tazemetostat, an EZH2 Inhibitor: Clinical Activity and Favorable Safety in Patients With Relapsed or Refractory B-Cell Non-Hodgkin Lymphoma*. in International Conference on Malignant Lymphoma. 2017. https://doi.org/10.1002/hon.2437_3
- Italiano, A., et al., *Tazemetostat, an EZH2 inhibitor, in relapsed or refractory B-cell non-Hodgkin lymphoma and advanced solid tumours: a first-in-human, open-label, phase 1 study*. The Lancet Oncology, 2018. **19**(5): p. 649-659.
- Chi, S., et al., *Abstract A175: Phase 1 study of the EZH2 inhibitor, tazemetostat, in children with relapsed or refractory INII-negative tumors including rhabdoid tumors, epithelioid sarcoma, chordoma, and synovial sarcoma*. Molecular Cancer Therapeutics, 2018. **17**(1 Supplement): p. A175-A175.
- Smith, S., et al., *Abstract CT029: The effect of tazemetostat on CYP3A-mediated metabolism of midazolam in patients with solid tumors*. Cancer Research, 2016. **76**(14 Supplement): p. CT029-CT029.
- Lin, J.H., *CYP induction-mediated drug interactions: in vitro assessment and clinical implications*. Pharm Res, 2006. **23**(6): p. 1089-116.
- Vaswani, R.G., et al., *Identification of (R)-N-((4-Methoxy-6-methyl-2-oxo-1,2-dihydropyridin-3-yl)methyl)-2-methyl-1-(1-(1-(2,2,2-trifluoroethyl)piperidin-4-yl)ethyl)-1H-indole-3-carboxamide (CPI-1205), a Potent and Selective Inhibitor of Histone Methyltransferase EZH2, Suitable for Phase I Clinical Trials for B-Cell Lymphomas*. J Med Chem, 2016. **59**(21): p. 9928-9941.
- Kung, P.P., et al., *Optimization of Orally Bioavailable Enhancer of Zeste Homolog 2 (EZH2) Inhibitors Using Ligand and Property-Based Design Strategies: Identification of Development Candidate (R)-5,8-Dichloro-7-(methoxy(oxetan-3-yl)methyl)-2-((4-methoxy-6-methyl-2-oxo-1,2-dihydropyridin-3-yl)methyl)-3,4-dihydroisoquinolin-1(2H)-one (PF-06821497)*. J Med Chem, 2018. **61**(3): p. 650-665.

18. CPI-1205 EC₅₀ = 28 nM and GI₅₀ = 436 nM; 1 EC₅₀ = 2.5 nM and GI₅₀ = 53 nM.
19. Stuckey, J.I. *Identification of high affinity, 2nd Generation EZH2 inhibitors using kinetic methods.* in *20th Annual Drug Discovery Summit* 2019. Berlin, Germany: Oxford Global.
20. Beno, B.R., et al., *A Survey of the Role of Noncovalent Sulfur Interactions in Drug Design.* Journal of Medicinal Chemistry, 2015. **58**(11): p. 4383-4438.
21. Hariparsad, N., et al., *Comparison of Immortalized Fa2N-4 Cells and Human Hepatocytes as in Vitro Models for Cytochrome P450 Induction.* Drug Metabolism and Disposition, 2008. **36**(6): p. 1046-1055.
22. We generally found that a cLogD of 3.3 or lower dampened expression of CYP3A4 to <5X under our assay conditions.
23. Knutson, S.K., et al., *Selective Inhibition of EZH2 by EPZ-6438 Leads to Potent Antitumor Activity in EZH2-Mutant Non-Hodgkin Lymphoma.* Molecular Cancer Therapeutics, 2014. **13**(4): p. 842-854.
24. Karanikolas, B.D.W., M.L. Figueiredo, and L. Wu, *Comprehensive evaluation of the role of EZH2 in the growth, invasion, and aggression of a panel of prostate cancer cell lines.* The Prostate, 2010. **70**(6): p. 675-688.
25. Antonarakis, E.S., et al., *AR-V7 and Resistance to Enzalutamide and Abiraterone in Prostate Cancer.* New England Journal of Medicine, 2014. **371**(11): p. 1028-1038.

Graphic entry for the Table of Contents (TOC):

